Histological and haematological analysis of the ascidian *Botrylloides leachii* (Savigny, 1816) during whole-body regeneration

Simon Blanchoud[1,2] (simon.blanchoud@otago.ac.nz), Lisa Zondag[1] (lisa.zondag@otago.ac.nz), Miles D. Lamare[3] (miles.lamare@otago.ac.nz) and Megan J. Wilson[1*] (meganj.wilson@otago.ac.nz)

[1]Department of Anatomy, Otago School of Medical Sciences; [3]Department of Marine Science, Division of Sciences; [1,3]University of Otago, P.O. Box 56, Dunedin 9054, New Zealand. [2] Present address: Department of Biology, University of Fribourg, Chemin du Musée 10, 1700 Fribourg, Switzerland.

*corresponding author: Ph. +64 3 4704695, Fax: +64 479 7254

Running title: *Botrylloides leachii* whole-body regeneration

Article type: Original paper

Abstract (250 words)

Whole-body regeneration, the formation of an entire adult from only a small fragment of its own tissue, is extremely rare among chordates. Exceptionally, in the colonial ascidian *Botrylloides leachii*, a fully functional adult is formed from their common vascular system, upon ablation of all adults from the colony, in just 10 days thanks to their high blastogenetic potential. While previous studies have identified key genetic markers and morphological changes, no study has yet focused on the haematological aspects of regeneration despite the major involvement of the remaining vascular system and the contained haemocytes in this process. To dissect this process, we analysed colony blood flow patterns using time-lapse microscopy to obtain a quantitative description of the velocity, reversal pattern, and average distance travelled by haemocytes. We also observed that flows present during regeneration are powered by temporally and spatially synchronized contractions of the terminal ampullae. In addition, we revised previous studies on *B. leachii* haematology as well as asexual development using histological sectioning, and compared the role of haemocytes during whole-body regeneration. We found that regeneration starts with a rapid healing response characterized by blood clotting and infiltration of immunocytes, followed by increased activity of haemoblasts, recruitment of macrophage-like cells for clearing the tissues of debris, and their subsequent disappearance from the circulation concomitant with the maturation of a single regenerated adult. Overall, we provide a uniquely detailed account of the haematological properties of regenerating *B. leachii* colonies, providing novel lines of inquiry towards the decipherment of regeneration in chordates.

Keywords: *Botrylloides leachii*, haemocytes, haemolymph flow, histology, whole-body regeneration

Introduction

Whole-body regeneration (WBR) is the process whereby an entire functional adult is formed from only a minute fragment of the original organism. Multicellular animals capable of varying degrees of regeneration are distributed widely throughout the metazoa (Sánchez Alvarado and Tsonis, 2006), thus suggesting that this biological phenomenon has a primordial origin. However, this regeneration ability correlates inversely with body and tissue complexity (Alvarado, 2000; Rinkevich et al., 2007).

Among vertebrates, while most adults heal only through scarring, the teleost fish and urodele amphibians can regenerate tissues, body parts or organs following injury (Jaźwińska and Sallin, 2016; Seifert et al., 2012; Tanaka and Reddien, 2011). While the study of these organisms has brought an extensive knowledge of patterning and cellular programs required for regeneration in mature animals following severe injury, no vertebrate has yet been shown to undergo WBR. Therefore, deciphering the mechanisms underlying regeneration in evolutionarily related organisms might provide new implications about the basic principles of cellular plasticity in adult organisms of our phylum.

Colonial tunicates represent the closest phylogenetic relative of vertebrates (Delsuc et al., 2006) and can undergo WBR due to their high blastogenetic potential (Oka & Watanabe, 1957, 1959; Milkman, 1967; Zaniolo et al., 1976; Rinkevich et al., 1995). Belonging to the Phylum Chordata, Class Ascidiacea, these invertebrates have tissue and organ complexity reminiscent of vertebrates (see Fig. 1), including a well-developed notochord, dorsal nerve cord, and a post-anal tail during their free-living tadpole larval stage. In particular, *Botrylloides leachii* (order Stolidobranchia, family Styelidae; Savigny, 1816) can undergo WBR in as little as 10 days (Rinkevich et al., 1995; Rinkevich et al., 2007, 2008, 2010; Zondag et al., 2016). Consequently, *B. leachii* has recently emerged as a model organism for the study of regeneration (Gross, 2007).

71 *B. leachii* are sessile suspension-feeding ascidians that live in clonal colonies of adults,
72 termed zooids, which organize in a series of ladder-like parallel rows, known as systems (Fig.
73 1 A-B; Brewin, 1946; Michaelsen, 1921; Savigny, 1816). The colony attaches to its substrate,
74 typically underneath rocks in the shallow subtidal zone, through a gelatinous tunic. While
75 each zooid has an independent heart and an open haemocoelic circulatory system, the entire
76 colony shares a common vascular system that is embedded in the tunic and closed at its
77 periphery by terminal ampullae, the contractile blind ends of marginal vessels (Fig. 1 C-F;
78 Mukai et al., 1978). *B. leachii* zooids are hermaphrodites and can reproduce both sexually, to
79 colonize new locations through a tadpole larval stage, or asexually, to expand the colony
80 (Berrill, 1947; Mukai et al., 1987). This latter reproduction, also known as palleal budding
81 (Oka and Watanabe, 1959) or blastogenesis (Brunetti, 1976), occurs on the outer epithelial
82 mantle of a zooid, typically on both of its sides thus producing two offspring. These growing
83 buds start as a thickened ring of cells on the body wall and invaginate to form the required
84 layers of tissue for organ development. Eventually, these buds, located on either side of the
85 older zooid, will mature into new adults (Berrill, 1947). As in the closely related genus
86 *Botryllus* (Berrill, 1941; Sabbadin, 1969), bud development is synchronous throughout the
87 colony and starts very early in the life cycle of the parent bud (Berrill, 1947; Brunetti, 1976).
88 In addition to these two methods of reproduction, *B. leachii* colonies can undergo WBR
89 from a minute fragment of their vascular tissue (~200 cells; Rinkevich et al., 1995). WBR will
90 only be triggered following the loss of all zooids from the colony; otherwise a more traditional
91 injury healing will occur (Rinkevich et al., 1995). *Botrylloides leachii* WBR starts with the
92 healing of the injury sites to prevent further haemolymph loss, followed by the compaction of
93 the marginal ampullae towards the centre of the remaining matrix. Within this reorganized
94 tissue, regeneration niches – a discrete regeneration locus within the vascular system – will
95 develop and compete through a yet undetermined process that ultimately leads to the

96 development of a single adult zooid, while all other niches are absorbed by the colony (Fig. 1
97 G). Importantly, WBR ability in *B. leachii* is retained throughout its developmental cycle (Oka
98 and Watanabe, 1959; Rinkevich et al., 2007), in contrast to the sister species *Botryllus*
99 *schlosseri*, where WBR potential is only present during a one-day period of their asexual
100 reproduction cycle, known as takeover (Rinkevich et al., 2008; Voskoboynik et al., 2007).
101 While the exact origin of the totipotent stem-like cells responsible for WBR remains unknown,
102 it has been shown that even though they will develop a regeneration niche within the vascular
103 system, they are not part of the circulating blood cells (haemocytes) in uninjured colonies but
104 rather appear to migrate from the vascular lining into the vascular system after injury
105 (Rinkevich et al., 2010).

106 Similar to most other chordates, ascidian haemocytes are continually renewed to
107 compensate for cell death and external sources of loss (Ermak, 1982). The location of
108 haemopoiesis in ascidians is still debated, which might be a consequence of the variety of
109 developmental strategies observed among this clade (Brown and Swalla, 2012). In some
110 solitary ascidians, it principally occurs in small static clusters of haemoblasts located in the
111 lining of the haemocoel, particularly around the pharyngeal basket (Ermak, 1982). In colonial
112 ascidians, clusters of undifferentiated cells with pluripotent properties, called islands, have
113 been detected in the sub-endostylar ventral sinus (Voskoboynik et al., 2008). In addition,
114 ventral islands located near the endostyle have been identified as sites of phagocyte turnover
115 (Lauzon et al., 2013). Furthermore, circulating haemoblasts have been shown to express
116 stemness and proliferation markers around early buds of *Botrylloides violaceus*, suggesting a
117 circulatory source of haemocytes (Brown et al., 2009). It thus appears that there may be
118 multiple sites for ascidian blood (haemolymph) production, in particular in colonial tunicates.

119 Haemolymph is mostly colourless and composed of a variety of cell types with
120 functions reminiscent to that of vertebrates (Cima et al., 2002; Goodbody, 1975; Millar and

121 Ratcliffe, 1989; Wright, 1981); and its flow patterns are intimately linked to the health of the
122 whole colony (Dijkstra et al., 2008).

123 Although there has been a number of studies investigating the morphotypes of
124 ascidian haemocytes (Ballarin et al., 2011; Ballarin and Cima, 2005; de Leo, 1992; Endean,
125 1960; Freeman, 1964; Hirose et al., 2003; Wright and Ermak, 1982), including of *B. leachii*'s
126 (Cima et al., 2002), improved resolution and colour images would benefit future work on this
127 species. In addition, no common terminology has been accepted to identify these cell types,
128 mainly because of discrepancies between their phenotype and their function in different
129 species, as well as a lack of understanding of their differentiation lineages (Ballarin et al.,
130 2011; Cima et al., 2002; Endean, 1960; Freeman, 1964; Goodbody, 1975; Millar and Ratcliffe,
131 1989; Wright, 1981). Furthermore, accurate identification is crucial for detecting and
132 interpreting variations in the sub-populations of haemocytes during WBR.

133 Despite the major involvement of the remaining vascular system and the comprised
134 haemocytes during WBR in *B. leachii*, no study has yet focused on the haematological aspects
135 of regeneration. To obtain a more accurate understanding of the WBR process in *B. leachii,* we
136 set out to characterize in a consistent and amended approach both uninjured and
137 regenerating colonies at the circulatory, tissue, and cellular levels. We used both histological
138 staining and time-lapse recording to dissect this highly dynamic process of regeneration with
139 greater resolution.

Materials and Methods

Animal husbandry and manipulation

Botrylloides leachii colonies were collected from the two sites in the Otago Harbour (45°52'12''S, 170°31'48''E and 45°49'41''S, 170°38'29''E), and Nelson Harbour (41°15'36''S, 173°16'48''E), New Zealand between September and March over 2014 to 2016. *B. leachii* grows naturally on submerged structures (e.g. ropes, pontoons, tyres), and colonies were removed from the attached substrata with a single edge razor blade. Each colony was placed on either 5.0 x 7.5-cm or 2.6 x 7.6-cm glass slides and left horizontally for two days in 200 ml of still seawater, changed daily, to allow the colony to attach to the slide. The slides were then placed vertically and kept at the Portobello Marine Laboratory (University of Otago) in a tank supplied with a constant flow-through of filtered seawater directly from the harbour, with temperature controlled between 18 °C and 20 °C. The glass slides were kept clear of algal growth by using a paintbrush and a single edge razor blade (after Rinkevich et al., 2007). Colonies were continuously fed, using a peristaltic pump, a 1:1:1:1 by volume mixture of three algae (*Chaetoceros muelleri*, *Pavlova lutheri* and *Tetraselmis chuii*) and a rotifer (*Brachionus plicatilis*) culture, complemented with Alltech All-G-Rich algae/yeast powder mix (12 g of Alltech All-G-Rich were added each week to the rotifer culture).

B. leachii haemolymph was collected as previously described (Cima, 2010). Briefly, whole colonies were first cleaned using filtered seawater (FSW) and incubated for 5 min in anticoagulant solution (0.38 g sodium citrate per 100 ml FSW, pH 7.5). To prevent loss of haemocytes, all instruments were incubated twice for 1 min in the anticoagulant solution prior to collection. Colonies were then dried using blotting paper and their marginal vessels broken using a needle. The haemolymph was then collected using a syringe and transferred into a 1.5-ml microfuge tube containing 100 µl of the anticoagulant solution up to a total volume of 600 µl. The tube was left 5 min on ice and the supernatant transferred to a new

tube to remove debris. Following centrifugation at 780 g for 12 min, the supernatant was discarded and the pellet re-suspended in 100 µl FSW.

B. leachii regeneration was carried out following an established protocol (Rinkevich et al., 2007). Dissection of adults and buds away from the marginal ampullae, during their mid-cycle blastogenic stage (i.e. not undergoing take-over), was carried out using a scalpel and a single edge razor blade. The slides with the remaining vascular fragments were then placed into an aerated seawater tank at 19 °C and left to regenerate until a certain morphological stage had been reached.

Histological staining

B. leachii regenerating tissue fragments were fixed overnight in 4% paraformaldehyde (PFA) in FSW, dehydrated in 70 % ethanol (EtOH) and embedded in paraffin wax. The fragments were then sectioned (5 µm thickness*)* in the transverse plane. Three stains were used on dewaxed slides: haematoxylin and eosin (H&E), Giemsa, and Martius Scarlet Blue trichrome (MSB). H&E staining was performed as follows: stain for 4 min in haematoxylin (Leica Biosystems Surgipath Gill II Haematoxylin), wash for 2 min in running tap water, place the slide for 2 min in Scott's tap water (2 g of potassium bicarbonate, 20 g magnesium sulphate per litre), wash again for 2 min, stain for 30 s in eosin (Leica Biosystems Surgipath Eosin), wash for 1 min, dehydrate and mount. Giemsa staining was performed as follows: stain for 30 min in a coplin jar containing Giemsa (7.36 g Giemsa powder in 500 ml of 50 °C glycerol and 500 ml methanol, mix 1:45 in dH_2O) within a 56 °C waterbath, rinse in dH_2O, differentiate in 1/1500 acetic acid solution, rinse in dH_2O, dehydrate and mount. MSB staining was performed as follows: stain for 5 min in Celestine blue (5 g ferric ammonium sulphate, 0.5 g Celestine Blue B in 100 ml dH_2O with 14 ml glycerol), wash for 30 s in running tap water, stain for 5 min in haematoxylin, wash again for 2 min, place the slide for 2 min in Scott's tap

water, wash for 2min, rinse for 1min in 95 % ethanol, stain for 2 min in martius yellow (20 g phosphotungstic acid, 5 g martius yellow per litre of 95 % ethanol), rinse three times for 1 min in dH_2O, stain for 10 min in brilliant scarlet (10 g brilliant scarlet crystal ponceau 6R, 20 ml glacial acetic acid per litre of dH_2O), rinse again three times, place the slide for 4 min in phosphotungstic acid (10 g per litre of dH_2O), rinse for 1 min in dH_2O, stain for 45 s in methyl blue (5 g methyl blue, 10 ml glacial acetic acid per litre of dH_2O), rinse for 1 min in acetic acid (10 ml glacial acetic acid per litre of dH_2O), dehydrate and mount.

Haemolymph smears were obtained as previously described (Cima, 2010). Briefly, drops of 50 µl of isolated haemocytes (see above) were left for 30 min to attach on SuperFrost Plus (Thermo Fisher Scientific) microscopy slides. The drop was then discarded by placing the slide vertically and the remaining attached cells were fixed for 30 min at 4 °C in ascidian fixative solution (1 g NaCl and 1 g sucrose in 1 % glutaraldehyde in FSW). Slides were then rinsed for 10 min in 0.1 M PBS, stained using 10 % Giemsa, mounted using a 9:1 glycerol-PBS solution and sealed with a coverslip using nail polish..

Imaging

All fixed samples were imaged on an Olympus AX70 microscope equipped with a QImaging MicroPublisher 5.0 2560 x 1920 pixels camera using QCapture. Magnification used ranged from 4 x to 100 x. Time-lapse recordings of haemolymph flow in live colonies were acquired on a Leica M205 FA stereo-microscope equipped with an 8 megapixel CCD DFC490 colour camera using the Leica Application Suite (LAS). Recordings were acquired using the "Movie" continuous mode, at different magnifications (7.42 x to 20 x) and exposure times (27.7 ms to 55.7 ms) adapted to the recorded portions of the colony, with a resolution of either 544 x 408 or 1088 x 816 pixels.

215 **Data processing**

216 Acquired images were processed for colour balance using the open-source Gimp
217 program (www.gimp.org) and assembled into figures using the open-source Inkscape
218 software (www.inkscape.org). Colours were chosen according to the ColorBrewer palette
219 (www.colorbrewer2.org). Movies were montaged using the Lightworks program
220 (www.lwks.com) and compressed using the open-source HandBreak tool
221 (www.handbreak.fr).

222 Haemolymph composition during WBR was estimated by manually identifying cell
223 types in microscopy images using five randomly located images of Giemsa stained ampullae,
224 at a 60-x magnification. Similarly, 10 images were used to characterize haemolymph
225 composition in intact colonies fixed during their mid-cycle blastogenic stage. Only cells
226 located inside the ampullae, centred on the imaged section and unambiguously identified
227 (2.6 % of the total 2339 cells could not be determined) were considered. Between 272 and
228 447 cells were positively identified for each stage of regeneration, 502 for the intact colony.
229 We focused our counting on ampullae for setting up a meaningful comparison between intact
230 and regenerating tissues as blood vessels become very sparse after tissue contraction (i.e.
231 stage 3, see Fig. 5).

232 The appearance of haemocytes was characterized using light microscopy by smearing
233 ascidian haemolymph and by staining histological sections of whole colonies.

234

235 **Computational analysis**

236 Vessel identification in time-lapse recordings was performed as follows. Raw frames
237 (Fig. S1 A) of the recording were smoothed using a Gaussian kernel of radius 0.89 μm, the
238 difference between consecutive frames was computed (Fig. S1 B) and moving cells were
239 identified as having an absolute value greater than 6 x the estimated standard deviation of the

image's white noise (Fig. S1 C; Paul et al., 2010). Cells larger than 5 μm^2 were then consecutively morphologically dilated and eroded, using structuring disks of radii 41 µm and 21 µm, respectively. The resulting detections were then averaged over the entire recording (Fig. S1 D), and vessels defined as containing moving cells in at least 30 % of the frames (Fig. S1 E). The location, length and width the vascular systems were then identified using the morphological skeleton of the vessels (Fig. S1 F).

Haemolymph flow was measured using a particle image velocimetry (PIV) approach with multiple passes and subpixel resolution using Fourier-space (Liao and Cowen, 2005) based on the difference between consecutive frames. Raw frames of the recording were smoothed using a Gaussian kernel of radius 0.89 µm, the difference between consecutive frames was computed (Fig. S1 G-I) and PIV performed between two consecutive differences, using a modified version of `matpiv_nfft` from the MatPIV toolbox (http://folk.uio.no/jks/matpiv/index2.html), through four consecutive passes with interrogation windows of sizes 83 x 83, 62 x 62, 41 x 41 and 21 x 21 µm; and finalized with a subpixel pass in Fourier-space (Fig. S1 J & K). Only the speeds measured inside the previously detected vessel segments were retained and projected onto the tangent of the segment. The orientation of each segment was then adjusted based on the maximal correlation between average speeds. Speeds from all aligned segments were then binned into a 2D histogram of resolution 350 ms x 6 µm/s, and the most likely haemolymph flow was computed using a shortest path approach (Dijkstra, 1959), implemented using dynamic programming (Fig. S1 L; Bellman, 1952). Finally, to dampen the effect of the binning required by dynamic programming, the resulting haemolymph flow was smoothed using cubic smoothing splines (Fig. S1 L).

Ampullar contractions were measured as follows. We first identified ampullae in every frame (Fig. S2 A) as regions darker than 20 x the estimated standard deviation of the image's

white noise (Paul et al., 2010). The resulting binarized image was then consecutively morphologically opened and closed, using a structuring disk of radius 9.5 µm (Fig. S2 B). The area and the centroid of each separated object was computed (Fig. S2 C), and the trajectory of each ampulla was reconstructed by clustering across frames detections whose centroids were closer than 19 µm (Fig. S2 D). Only trajectories that spanned more than 95 % of the frames were kept for further analysis. All the code written for our analysis was implemented as a set of custom MATLAB R2015b (MathWorks) functions and is available upon request.

Results

Haemolymph circulation

As a first step towards dissecting WBR, we characterized the haematological properties of a healthy and intact adult colony of *B. leachii* (Fig. 1 A-B). Haemolymph circulation in suspension-feeding ascidians undergoes a periodic reversal of flow direction between advisceral (towards the viscera) and abvisceral (towards the branchial basket). The advisceral flow starts on the anterior side of the heart, moves towards the endostyle before arriving to the pharynx and the mid-dorsal vessel, which supplies haemolymph to the digestive tract, and lastly passes to the dorsal end of the heart (Mukai et al., 1978).

Utilising the transparency of the tunic, we recorded time-lapse stereomicroscopy data from eight colonies at different locations in their vascular system (Fig. 1 C-F, Movies S1). Focusing on the largest vessels of the colony (Movie S1-S2), we gathered a set of reproducible flow measurements (n=9, from 5 different colonies) that allowed us to calculate, using a custom-made PIV-based tracking software, the flow (peak velocity ~200µm/s) and reversal rates (~57/24 s) of a *B. leachii* colony (Fig. 2 A & Fig. S1).

When recording vascular junctions, we observed (Movie S1) and quantified (Movie S3) an apparently pseudo-erratic pattern at the time of flow reversal. By examining terminal vessels (Movie S1), we extracted valuable information on the rate (11.4 ± 5.3 $\mu m^2/s$, n=18) and extent (dilated/contracted surface ratio: 1.55 ± 0.26, n=12) of the ampullar contraction-dilatation cycle concomitant with haemolymph flow in ascidians (Mukai et al., 1978). While the general timing of haemolymph and ampullae alternation is synchronized (average lag: 2.9 ± 2.5 s, n=24), small variations on the exact time of contraction for each ampulla could be measured (± 3.1 s, n=24, Fig. 2 B & Fig. S2).

Haemocyte classification

297 By combining previous classification schemes for botryllid ascidians (Ballarin et al.,
298 2011; Ballarin and Cima, 2005; Cima et al., 2002; Hirose et al., 2003), we propose a
299 generalized classification of *B. leachii* circulatory haemocytes into five functional groups:
300 undifferentiated cells, immunocytes, mast cell-like cells, transport cells and storage cells
301 (Table 1). A further detailed description of the observed cell types is provided in Table S1. In
302 this classification, undifferentiated cells are composed solely of haemoblasts, also called
303 lymphocytes or lymphocyte-like cells. Immunocytes can be further classified between
304 phagocytes and cytotoxic cells. Phagocytes include hyaline amoebocytes and macrophage-like
305 cells while cytotoxic cells include granular amoebocytes and morula cells. Mast-like cells are
306 represented only by granular cells. Transport cells are composed of compartment
307 amoebocytes and compartment cells. Finally, storage cells include both pigment cells and
308 nephrocytes. A comprehensive guide to haemocyte identification using bright field Giemsa
309 stained images is provided (Table 2), with high magnification pictures exemplifying the most
310 common aspect of each cell type (Fig. 3).

311 Altogether, these descriptions (Table 2) and images (Fig. 3) allowed us to identify most
312 of the cells both in haemolymph smears and histological sections and provide an
313 unambiguous identification reference for the analysis of the localization and fate of *B. leachii*
314 haemocytes in the colony.

315

316 **Asexual budding**

317 To obtain a precise picture of the prevailing mode of asexual reproduction, we revised
318 various stages of blastogenesis in *B. leachii* previously described by Berrill (1941, 1947) using
319 histological sections. Palleal reproduction involves the formation of a new bud from the
320 peribranchial epithelium of a zooid. Remarkably, in *B. leachii* as well as in other colonial
321 botryllid, because blastogenesis starts very early in the development of a maturing bud, there

322 are typically three generations co-existing in the colony (Fig. 4 A): second-generation buds
323 (budlets), developing from more differentiated buds (first-generation buds), themselves
324 attached to adult filter-feeding zooids (blastozooids).

325 The first visible sign of blastogenesis is the appearance of a bud disc, a thickened disk
326 of cells on the ventral side of the atrial epithelium of a first-generation bud, just before the
327 stage where its stigmata become perforated. In healthy colonies, one bud disc usually appears
328 on each side of the forming pharyngeal basket (Fig. 4 B), thus producing two budlets and
329 increasing the overall size of the colony. In well-fed colonies, one of these buds can even
330 divide to give rise to two buds on one side of the zooid, producing one further zooid (Berrill,
331 1947). The disc cells then proliferate until the bud reaches around 12 cells of diameter (day 1
332 of the second-generation development), protrudes outside of the first-generation bud through
333 its mantle into the tunic (Fig. 4 C) and curves to form a hollow sphere of cells inside a mantle
334 pouch highly reminiscent of the early stages of blastogenesis (days 2-3). This pouch connects
335 the growing bud with the haemocoel of the mother bud, ensuring that haemolymph and
336 oxygen reach the new bud while the rudiment for the vascular connection to the rest of the
337 colony will be initiated underneath by an outgrowth of the epithelium layer (Berrill, 1947),
338 later producing the radial vessel (Burighel and Brunetti, 1971).

339 The asexually developing bud continues to increase in size and begins to fold, forming
340 three main compartments, which will form the internal structures of the new adult (days 4-6,
341 Fig. 4 D). It is at that stage that the first signs of germ cells can also be observed (Fig. 4 D). The
342 folds will ultimately join, creating the basic structure for the pharyngeal basket (days 7-8).
343 Once the extending pharyngeal basket has joined the stomach and started to produce its first
344 imperforated stigmata, the stereotypical body plan of the zooid is completed, thus becoming a
345 first-generation bud on which new budlets start to appear (day 9, Fig. 4 E). Following this
346 stage, the first-generation bud will differentiate into a fully functional zooid hence growing in

size, finalizing its various organs and vascular system (days 10-22, Fig. 4 F), starting its cardiac activity around day 17.

In total, it takes approximately 22 days at 17 °C to produce a functioning zooid through blastogenesis (Berrill, 1947). Afterwards, the zooid will feed for another 8 days before it gets resorbed through a whole-body apoptosis (< 3 days), in which numerous large macrophage-like cells infiltrate and remove effete cells from the senescent tissues (Brunetti, 2009) and the next generation succeeds.

B. leachii whole-body regeneration

The vascular and haematological characteristics of WBR in *B. leachii*, are described through comparisons with blastogenesis and intact colonies (Fig. 5). For this analysis, we follow a published classification of WBR into 5 stages (Fig. 1 G; Zondag et al., 2016): Stage 0, injury of the colony; Stage 1, healing of the injury; Stage 2, remodelling of the vascular system; Stage 3, condensation of the ampullae; Stage 4, establishment and development of regeneration niches; Stage 5, fully regenerated zooid.

Stage 0: Injury (0 h)

B. leachii has a great capacity for preventing haemolymph loss from injuries, with haemolymph loss stopped in less than 30 s by a combination of tissue contraction and clotting (Movie S4). Upon ablation of the zooids, the remaining vascular tissue initially looses a small volume of haemolymph but quickly contracts its peripheral vessels to halt the oozing and starts clotting (Fig. 5 A). Flow will then restart after a pause, the duration of which is seemingly related to either the number of ampullae or the amount of vascular tissue, but was consistently shorter than 10 min. We observed restart of haemolymph flow in as little as two minutes (Movie S4), starting in the portion of the tissue furthest away from the injury in an

372 erratic yet bidirectional fashion, and progressively re-spanning almost the entire vascular
373 system (Movie S4). Although driven only by ampullar contractions, this novel haemolymph
374 flow exhibits a reversal frequency similar to that of intact vessels in a whole colony. As
375 suspected, given the short amount of time available for new cellular differentiation, the
376 composition of this haemolymph is almost identical to the one from intact colonies, with a
377 slight increase in the population of granular cells (Fig. 5 G).
378
379 *Stage 1: Wound healing (15 h)*
380 At this stage of WBR, a dramatic amount of extravascular cellular activity is taking
381 place. The two most apparent aspects are the infiltration of morula cells into the tunic and the
382 remodelling of the tunic matrix (Fig. 5 B). When focusing on circulating haemocytes, we
383 observed an incipient decrease in the population of morula cells, accompanied with an
384 increase in the populations of haemoblasts, hyaline amoebocytes, and granular cells (Fig. 5 G).
385
386 *Stage 2: Ampulla remodelling (24 h)*
387 Concomitant with the observed wound healing process, terminal ampullae start
388 changing their elongated shape to a more spheroid form, contracting, and creating novel tunic
389 vessels (Fig. 5 C; Rinkevich et al., 1995; Rinkevich et al., 2007). One day after injury,
390 previously reported giant cells (Rinkevich et al., 1995, 2007) could be observed throughout
391 the vascular system (Fig. 5 C). In addition, this step exhibits the first signs of the subsequent
392 increase in phagocytic cells (Fig. 5 G).
393
394 *Stage 3: Tissue contraction (2 - 4 d)*
395 By stage 3, the vascular system had fully contracted into a dense network (Rinkevich et
396 al., 1995, 2007) and various regeneration niches were visible within the tissue (Fig. 5 D).

Regeneration niches are defined as spherical aggregates of cells within the vascular lumen. Probably the most striking change, at this stage of WBR, was the large increase in phagocytic cells (Fig. 5 D & G), while numbers of both haemoblasts and differentiating cells had returned to pre-injury levels (Fig. 5 G).

Stage 4: Regeneration niches (5 - 7 d)

During stage 4, several regeneration niches were present and the foundation of an adult could be observed within one of them (Fig. 5 E). Nonetheless, only one zooid will regenerate and the less developed niches will be resorbed (Rinkevich et al., 1995, 2007). Advanced niches already displayed well developed axial and tissue organizations reminiscent of the early first-generation stage of blastogenesis (Fig. 4 E), including an endostyle as well as an imperforated pharyngeal basket (Fig. 5 E). In comparison to palleal budding, the regenerating buds were lacking both an interstitial space around the niche and visible gametes (compare Fig. 4 E and Fig. 5 E).

At this stage of WBR, haemolymph flow can be observed in novel tunic vessels (Movie S5), and the composition of the haemolymph strives towards the composition observed in intact colonies. Transport, mast-cell like, and storage cells are at their lowest during this period while hyaline amoebocytes and macrophage-like cells remain at a higher proportion than in uninjured colonies (Fig. 5 G).

Stage 5: Regenerated zooid (8 - 10 d)

At the conclusion of WBR, a single fully functional zooid is regenerated, displaying the palleal buds expected from an uninjured adult (Fig. 5 F). The haemolymph composition of this new adult is largely similar to that of an intact colony, albeit with a slightly smaller phagocytic cell population (Fig. 5 G).

Discussion

Here, we carefully dissected the haematological and histological properties of both intact and regenerating *B. leachii* colonies. We compared haemolymph flow patterns to published data from related ascidian species and revised previous studies on *B. leachii* asexual development. In addition, we followed the quantity and location of each type of haemocyte during whole-body regeneration, finding that regeneration progresses through a rapid healing response, an increased activity of haemoblasts, the recruitment of macrophage-like cells and finally their clearing from the haemolymph.

Synchronization of blood flow in intact and regenerating colonies

Using time-lapse recording, we were able to quantify the complex haemolymph flow patterns observed within a *B. leachi* colony. While the velocity of haemolymph in ascidians has to our knowledge not yet been estimated, the measured average velocity predicts that haemocytes travel an average of 8 mm during one alternation of the flow. In such a small organism (~2 mm in length), this range could be critical for spreading signalling metabolites and thus potentially coordinating colony responses. The values we obtained for the reversal rates are similar to those measured in other ascidian species, albeit slightly more asymmetric and with a relatively shorter advisceral period (21 to 36 s in *B. leachi*, 30 to 50 s in *Botryllus primigenus* and 45 to 60 s in *Symplegma reptans*; Mukai et al., 1978). We also observed a quick reestablishment of a regular haemolymph flow after injury, and despite the removal of all zooids from the vascular system. This flow is thus sustained solely by synchronized and localized patterns of ampullar contractions (Fig. 2 C & Fig. S3, Movie S4-S5). While this synchronization could solely be a consequence of haemolymph pressure and elastic vascular

446 tissue (Mukai et al., 1978), the absence of any zooid heart within the tunic suggests the
447 existence of a yet unidentified stimulus coordinating this activity.

448 Similar to vertebrates (Miquerol and Kelly, 2013), *B. leachii* heart activity starts before
449 the zooid is fully mature, when neither capable of filter feeding nor of using most of its other
450 organs. Early heart function is consistent with the necessity to circulate oxygen and nutrients
451 throughout the developing organism, even though the parental heart is connected directly to
452 the haemocoel of the bud and would appear to be sufficient for sustaining such circulation. In
453 fact, the pressure exerted by the parental heart is strong enough to impose its direction and
454 reversal rate onto the daughters' heart (Burighel and Brunetti, 1971).

455

456 **Morphological and cellular changes during distinct phases of *B. leachii* WBR**

457 We additionally characterised the morphological and haematological modulation of
458 injured colonies throughout WBR. Morula cells are known constituents of the immune system
459 involved in inflammatory responses, haemolymph clotting, homeostasis, and tunic repair
460 (Ballarin et al., 2011, 2001; de Leo, 1992; Menin et al., 2005). The large number of infiltrated
461 morula cells observed during stage 1 of WBR highlights a need for both clearance of decaying
462 or foreign debris and reorganization of the injured vascular system during the first 15 h post
463 dissection. In addition, we measured an increase in the population of differentiating cells
464 (Fig. 5 G), consistent with the need to re-establish homeostasis within the *B. leachii*
465 vasculature and to compensate for haemolymph loss. An increased number of mast cell-like
466 cells, a cell type apparently absent from related ascidian species (Cima et al., 2002), was also
467 observed. While their role remains unclear, two hypothesis have been proposed: either a
468 source of nourishment or the immunosurveillance of the alimentary tract (Cima et al., 2002).
469 Their presence during WBR, in the absence of any feeding zooid, rather supports a nutritive
470 role.

471 At stage 2, we observed the first signs of the subsequent increase in phagocytic cells,
472 potentially as a result of the previously observed differentiation activity (Fig. 5 G) and of the
473 inflammatory response induced by the morula cells (Fig. 5 B). Given the role of these
474 macrophage-like cells in the removal of foreign elements from the tissue (de Leo, 1992), their
475 presence during stage 3 of WBR points towards a recruitment for undertaking the clearing of
476 bacteria, dead cells, and residues of remodelled tunic. The concomitant reduction of
477 haemoblasts to pre-injury levels suggests that the wound healing and remodelling phase has
478 been completed, and that cellular proliferation as well as differentiation have returned to
479 haemopoietic levels within the vascular system. Finally, during stage 4, mast cell-like,
480 transport, and storage cells were observed at their lowest level throughout WBR. This could
481 be a direct consequence of the imposed absence of feeding, leading to a lack of nutrients to be
482 transported or stored. Regenerating *B. leachii* colonies would then need to obtain nutrients in
483 an alternative way. Similar to reactivation of hibernating colonies (Burighel et al., 1976) and
484 to the takeover of a new generation of buds in *Botryllus schlosseri* (Lauzon et al., 2002),
485 extraction of reserve nutrients from macrophage-like cells would supplement this need and
486 gradually reduce the number of phagocytic cells, as observed experimentally (Fig. 5 G).

487 When focusing on vascular circulation, the initial rapid interruption in haemolymph
488 flow (Movie S4) could be a consequence of either the reduced density of haemolymph inside
489 the vascular system, or an actively regulated mechanism to reduce the pressure at the
490 sectioned vessels and aiding clotting. Given that haemolymph flow restarts over a relatively
491 short time scale compared to that necessary for substantial haemocytes production and
492 pressure increase, the latter hypothesis appears more likely. This observation thus further
493 supports the existence of an unidentified stimulus systemic to the entire vascular system,
494 potentially relayed directly by the epithelial cells lining the vasculature (Mukai et al., 1978).

In our histological samples, we have observed a detachment of the vascular lining throughout, including in intact colonies (Fig. S4). This suggests that this detachment phenomenon, which has been described as the initial establishment of a regeneration niche (Rinkevich et al., 2007), is either a symptom of vascular remodelling that takes place naturally in healthy colonies but was somehow not prominent in our regenerating vascular tissues, or an artefact of the fixation procedure. Given that we did not consistently detect the reported precursory accumulation of haemocytes at the vascular lining, the latter hypothesis appears more likely, and we suggest that these peripheral cells are morula cells responding to an inflammatory response at the early stages of infiltration.

Similarities and divergences between blastogenesis and WBR

The two major discrepancies between these two processes were the absence during WBR of an interstitial space around the niche and a lack of visible gametes (Fig. 5 E). As WBR restores both the soma and the germ line (Rinkevich et al., 1995, 2007), the absence of gametes in regenerating niches indicates that they will be created during subsequent cycles of blastogenesis. This process may be an energetically economical developmental approach that avoids the production of gametes in niches that could subsequently be resorbed. Overall, once the vascular tissue has fully contracted, the timing of WBR initially relates closely to that of blastogenesis (day 1-8), but ultimately produces a functional adult much faster. One potential cause for such increased speed is the temperature at which the regenerating colonies were kept (~19 °C in the present study), which is known to directly correlate with developmental pace (Berrill, 1947, 1941). Temperature alone may not entirely explain such difference in timing however, and one likely cause could be that functional regenerated zooids are smaller than palleal ones, thus having a shortened growth phase which normally spans more than half

519 of blastogenesis. Indeed, such reduction in zooid size was observed in *Botryllus schlosseri*
520 (Voskoboynik et al., 2007).
521
522 **Conclusion**
523 Overall, this study underlines the complex interplay of mechanisms required for
524 successful WBR, and complements previous morphological studies (Rinkevich et al., 1995,
525 2007) by providing a higher temporal resolution. Our histological analysis of WBR supports
526 our recent sequencing approach that identified an initial healing phase followed by a
527 regeneration response (Zondag et al., 2016) and have provided the first detailed account of
528 the haematological properties of *Botrylloides leachii* colonies throughout whole-body
529 regeneration.

Compliance with Ethical Standards

Conflict of Interest: The authors declare that they have no conflict of interest. Informed consent was obtained from all individual participants included in the study. All applicable international, national, and/or institutional guidelines for the care and use of animals were followed. All permissions required for this study have been obtained.

Acknowledgements

We would like to thank Francesca Cima (Department of Biology, University of Padova) for pieces of advice, protocols and general help on haemocytes, as well as for proofreading this article; Rueben Pooley (Department of Marine Science, University of Otago) for his help in animal husbandry; Lorryn Fisher (Department of Anatomy, University of Otago) for providing the PCNA antibody; Noel Jhinku (Department of Pathology, University of Otago) for providing the rotifers; Kendall Gadomski (Department of Marine Science, University of Otago) for providing the All-G-Rich powder; Kristian Sveen (Institute for Energy Technology, University of Oslo) for developing the original code of MatPIV; Cynthia A. Brewer (GeoVISTA Center, Pennsylvania State University) for developing ColorBrewer; Fernando Romero Balestra (Department of Cell Signalling, CABIMER), Aude Blanchoud and Anna Jaźwińska (Department of Biology, University of Fribourg), for proofreading this article.

The project was supported by a Dean's Bequest Grant and by the Department of Anatomy [Otago University]; S.B. by the Swiss National Science Foundation (SNSF) [grant number P2ELP3_158873]; and L.Z. by a University of Otago Post-graduate scholarship.

References

Alvarado, A.S., 2000. Regeneration in the metazoans: why does it happen? BioEssays 22, 578–590. doi:10.1002/(SICI)1521-1878(200006)22:6<578::AID-BIES11>3.0.CO;2-#

Ballarin, L., Cima, F., 2005. Cytochemical properties of *Botryllus schlosseri* haemocytes: indications for morpho-functional characterisation. Eur. J. Histochem. 49, 255–64. doi:10.4081/952

Ballarin, L., del Favero, M., Manni, L., 2011. Relationships among hemocytes, tunic cells, germ cells, and accessory cells in the colonial ascidian *Botryllus schlosseri*. J. Exp. Zool. Part B Mol. Dev. Evol. 316B, 284–295. doi:10.1002/jez.b.21400

Ballarin, L., Franchini, A., Ottaviani, E., Sabbadin, A., 2001. Morula cells as the major immunomodulatory hemocytes in ascidians: Evidences from the colonial species *Botryllus schlosseri*. Biol. Bull. 201, 59–64. doi:10.2307/1543526

Bellman, R., 1952. On the theory of dynamic programming. Proc. Natl. Acad. Sci. U. S. A. 38, 716–9.

Berrill, N.J., 1947. The developmental cycle of Botrylloides. Q. J. Microsc. Sci. 88, 393–407.

Berrill, N.J., 1941. The development of the bud in Botryllus. Biol. Bull. 80, 169. doi:10.2307/1537595

Brewin, B.I., 1946. Ascidians in the vicinity of the Portobello Marine Biological Station, Otago Harbour. Trans. R. Soc. New Zeal. 76, 87–131.

Brown, F.D., Keeling, E.L., Le, A.D., Swalla, B.J., 2009. Whole body regeneration in a colonial ascidian, *Botrylloides violaceus*. J. Exp. Zool. B. Mol. Dev. Evol. 312, 885–900. doi:10.1002/jez.b.21303

Brown, F.D., Swalla, B.J., 2012. Evolution and development of budding by stem cells: Ascidian coloniality as a case study. Dev. Biol. 369, 151–162. doi:10.1016/j.ydbio.2012.05.038

Brunetti, R., 2009. Botryllid species (Tunicata, Ascidiacea) from the Mediterranean coast of Israel, with some considerations on the systematics of Botryllinae. Zootaxa 2289, 18–32.

Brunetti, R., 1976. Biological cycle of *Botrylloides leachi* (Savigny) (Ascidiacea) in the Venetian lagoon. Vie Milieu XXVI, 105–122.

Burighel, P., Brunetti, R., 1971. The circulatory system in the blastozooid of the colonial ascidian Botryllus Schlosseri (Pallas). Bolletino di Zool. 38, 273–289. doi:10.1080/11250007109429158

Burighel, P., Brunetti, R., Zaniolo, G., 1976. Hibernation of the colonial ascidian Botrylloides leachi (Savigny): histological observations. Ital. J. Zool. 43, 293–301. doi:10.1080/11250007609430146

Cima, F., 2010. Microscopy methods for morpho-functional characterisation of marine invertebrate haemocytes. Microsc. Sci. Technol. Appl. Educ. 1100–1107.

Cima, F., Perin, A., Burighel, P., Ballarin, L., 2002. Morpho-functional characterization of haemocytes of the compound ascidian *Botrylloides leachi* (Tunicata, Ascidiacea). Acta Zool. 82, 261–274. doi:10.1046/j.1463-6395.2001.00087.x

de Leo, G., 1992. Ascidian hemocytes and their involvement in defence reactions. Bolletino di Zool. 59, 195–214. doi:10.1080/11250009209386669

Delsuc, F., Brinkmann, H., Chourrout, D., Philippe, H., 2006. Tunicates and not cephalochordates are the closest living relatives of vertebrates. Nature 439, 965–968. doi:10.1038/nature04336

Dijkstra, E.W., 1959. A note on two problems in connexion with graphs. Numer. Math. 1, 269–271. doi:10.1007/BF01386390

Dijkstra, J., Dutton, A., Westerman, E., Harris, L.G., 2008. Heart rate reflects osmostic stress levels in two introduced colonial ascidians *Botryllus schlosseri* and *Botrylloides violaceus*. Mar. Biol. 154, 805–811. doi:10.1007/s00227-008-0973-4

Endean, R., 1960. The blood-cells of the ascidian, Phallusia Mammillata. J. Cell Sci. s3-101, 177–197.

Ermak, T.H., 1982. The renewing cell populations of ascidians. Am. Zool. 22, 795–805. doi:10.1093/icb/22.4.795

Freeman, G., 1964. The role of blood cells in the process of asexual reproduction in the tunicate *Perophora viridis*. J. Exp. Zool. 156, 157–183. doi:10.1002/jez.1401560204

Goodbody, I., 1975. The physiology of ascidians. Adv. Mar. Biol. 12, 1–149. doi:10.1016/S0065-2881(08)60457-5

Gross, L., 2007. From one to many and back again: a systemic signal triggers tunicate regeneration. PLoS Biol. 5, e98. doi:10.1371/journal.pbio.0050098

Hirose, E., Shirae, M., Saito, Y., 2003. Ultrastructures and classification of circulating hemocytes in 9 botryllid ascidians (chordata: ascidiacea). Zoolog. Sci. 20, 647–656. doi:10.2108/zsj.20.647

Jaźwińska, A., Sallin, P., 2016. Regeneration versus scarring in vertebrate appendages and heart. J. Pathol. 238, 233–246. doi:10.1002/path.4644

Lauzon, R.J., Brown, C., Kerr, L., Tiozzo, S., 2013. Phagocyte dynamics in a highly regenerative urochordate: insights into development and host defense. Dev. Biol. 374, 357–73. doi:10.1016/j.ydbio.2012.11.006

Lauzon, R.J., Ishizuka, K.J., Weissman, I.L., 2002. Cyclical generation and degeneration of organs in a colonial urochordate involves crosstalk between old and new: A model for development and regeneration. Dev. Biol. 249, 333–348. doi:10.1006/dbio.2002.0772

609 Liao, Q., Cowen, E.A., 2005. An efficient anti-aliasing spectral continuous window shifting technique for PIV. Exp.
610 Fluids 38, 197–208. doi:10.1007/s00348-004-0899-7
611 Menin, A., Favero, M. Del, Cima, F., Ballarin, L., 2005. Release of phagocytosis-stimulating factor(s) by morula
612 cells in a colonial ascidian. Mar. Biol. 148, 225–230. doi:10.1007/s00227-005-0081-7
613 Michaelsen, W., 1921. Die Botrylliden und Didemniden der Nordsee und der zur Ostsee fuhrenden
614 Meeresgebiete. Wissenschaftliche Meeresuntersuchungen (Abteilung Helgoland) 14, 99–124.
615 Milkman, R., 1967. Genetic and developmental studies on *Botryllus schlosseri*. Biol. Bull. 132, 229.
616 doi:10.2307/1539891
617 Millar, D.A., Ratcliffe, N.A., 1989. The evolution of blood cells: facts and enigmas. Endeavour 13, 72–7.
618 doi:10.1016/0160-9327(89)90005-7
619 Miquerol, L., Kelly, R.G., 2013. Organogenesis of the vertebrate heart. Wiley Interdiscip. Rev. Dev. Biol. 2, 17–29.
620 doi:10.1002/wdev.68
621 Mukai, H., Saito, Y., Watanabe, H., 1987. Viviparous development in Botrylloides (compound ascidians). J.
622 Morphol. 193, 263–276. doi:10.1002/jmor.1051930305
623 Mukai, H., Sugimoto, K., Taneda, Y., 1978. Comparative studies on the circulatory system of the compound
624 ascidians, Botryllus, Botrylloides and Symplegma. J. Morphol. 157, 49–78. doi:10.1002/jmor.1051570105
625 Oka, H., Watanabe, H., 1959. Vascular budding in Botrylloides. Biol. Bull. 117, 340. doi:10.2307/1538913
626 Oka, H., Watanabe, H., 1957. Vascular budding, a new type of budding in Botryllus. Biol. Bull. 112, 225.
627 doi:10.2307/1539200
628 Paul, P., Duessmann, H., Bernas, T., Huber, H., Kalamatianos, D., 2010. Automatic noise quantification for confocal
629 fluorescence microscopy images. Comput. Med. Imaging Graph. 34, 426–434.
630 doi:10.1016/j.compmedimag.2010.04.001
631 Rinkevich, B., Shlemberg, Z., Fishelson, L., 1995. Whole-body protochordate regeneration from totipotent blood
632 cells. Proc. Natl. Acad. Sci. U. S. A. 92, 7695–9.
633 Rinkevich, Y., Paz, G., Rinkevich, B., Reshef, R., 2007. Systemic bud induction and retinoic acid signaling underlie
634 whole body regeneration in the urochordate *Botrylloides leachi*. PLoS Biol. 5, e71.
635 doi:10.1371/journal.pbio.0050071
636 Rinkevich, Y., Rinkevich, B., Reshef, R., 2008. Cell signaling and transcription factor genes expressed during
637 whole body regeneration in a colonial chordate. BMC Dev. Biol. 8, 100. doi:10.1186/1471-213X-8-100
638 Rinkevich, Y., Rosner, A., Rabinowitz, C., Lapidot, Z., Moiseeva, E., Rinkevich, B., 2010. *Piwi* positive cells that line
639 the vasculature epithelium, underlie whole body regeneration in a basal chordate. Dev. Biol. 345, 94–104.
640 doi:10.1016/j.ydbio.2010.05.500
641 Sabbadin, A., 1969. The compound ascidian *Botryllus schlosseri* in the field and in the laboratory. Pubbl Staz Zool
642 Napoli 37, 62–72.
643 Sánchez Alvarado, A., Tsonis, P.A., 2006. Bridging the regeneration gap: genetic insights from diverse animal
644 models. Nat. Rev. Genet. 7, 873–884. doi:10.1038/nrg1923
645 Savigny, J.-C., 1816. Mémoires sur les animaux sans vertèbres. Dufour, G., Paris. doi:10.5962/bhl.title.9154
646 Seifert, A.W., Kiama, S.G., Seifert, M.G., Goheen, J.R., Palmer, T.M., Maden, M., 2012. Skin shedding and tissue
647 regeneration in African spiny mice (*Acomys*). Nature 489, 561–5. doi:10.1038/nature11499
648 Tanaka, E.M., Reddien, P.W., 2011. The cellular basis for animal regeneration. Dev. Cell 21, 172–185.
649 doi:10.1016/j.devcel.2011.06.016
650 Voskoboynik, A., Simon-Blecher, N., Soen, Y., Rinkevich, B., De Tomaso, A.W., Ishizuka, K.J., Weissman, I.L., 2007.
651 Striving for normality: whole body regeneration through a series of abnormal generations. FASEB J. 21,
652 1335–44. doi:10.1096/fj.06-7337com
653 Voskoboynik, A., Soen, Y., Rinkevich, Y., Rosner, A., Ueno, H., Reshef, R., Ishizuka, K.J., Palmeri, K.J., Moiseeva, E.,
654 Rinkevich, B., Weissman, I.L., 2008. Identification of the endostyle as a stem cell niche in a colonial chordate.
655 Cell Stem Cell 3, 456–64. doi:10.1016/j.stem.2008.07.023
656 Wright, R.K., 1981. Urochordates, in: Ratcliffe, N.A., Rowley, A.F. (Eds.), Invertebrate Blood Cells. Volume 2.
657 Arthropods to Urochordates, Invertebrates and Vertebrates Compared. Academic Press, London, pp. 565–
658 626.
659 Wright, R.K., Ermak, T.H., 1982. Cellular defense systems of the protochordata, in: Phylogeny and Ontogeny.
660 Springer US, Boston, MA, pp. 283–320. doi:10.1007/978-1-4684-4166-6_8
661 Zaniolo, G., Sabbadin, A., Resola, C., 1976. Dynamics of the colonial cycle in the ascidian, *Botryllus schlosseri*. The
662 fate of isolated buds. Acta Embryol Exp 205–213.
663 Zondag, L.E., Rutherford, K., Gemmell, N.J., Wilson, M.J., 2016. Uncovering the pathways underlying whole body
664 regeneration in a chordate model, *Botrylloides leachi* using de novo transcriptome analysis. BMC Genomics
665 17, 114. doi:10.1186/s12864-016-2435-6
666
667

668 **Figure legends**

669

670

671 **Fig. 1 *Botrylloides leachii* schematic morphology and physiology.** Abbreviations: zooid (z),
672 system (y), tunic (c), vascular system (v), terminal ampullae (a), buccal siphon (p_b), atrial
673 siphon (p_a), oral tentacles (t), endostyle (e), pharyngeal basket (k), stigmata (g), neural
674 ganglion (n), heart (h), stomach (s), bud (b), dorsal sinus (u_d), ventral sinus (u_v). (**A**) Top-view
675 of a stereotypical colony composed of 72 zooids. Dashed-delimited area magnified in **B**. (**B**)
676 Top-view of a single zooid. Longitudinal plane (dashed) depicted in **C**. (**C**) Left lateral view of a
677 zooid. Abvisceral/advisceral haemolymph direction and contraction/dilatation of ampullae
678 are depicted using red/purple arrows, respectively. Dashed-delimited areas are exemplified
679 in **D**-**F**. *In vivo* stereo-microscopic images of a large vessel (**D**), vascular junction (**E**) and
680 terminal ampullae (**F**), taken from recordings showcased in Movie S1. (**G**) *B. leachii* WBR from
681 a fragment of vascular tissue through our five defined stages and the approximate time-line

682

683

684 **Fig. 2 Quantification of the haemolymph circulation in *B. leachii*.** (**A**) Average (n=8)
685 abvisceral haemolymph flow based on PIV measurement of time-lapse large vessel recordings.
686 Depicted are the individual recordings (thin grey lines), the recording utilized for Fig. S1
687 (thick grey line), the average velocity (red line) and standard deviation (light grey area). A
688 visual representation of the duration of abvisceral and advisceral phase durations is shown
689 (blue). (**B**) Dilatation-contraction cycles of eight terminal ampullae (Fig. S2) from a single
690 time-lapse recording. The raw data (darker line) is overlaid with a smoothed measurement
691 (lighter line), local maxima and local minima (down and up triangles, respectively). The
692 abvisceral phase of the haemolymph flow corresponds to the contraction phase of the

693 ampullae. (**C**) Ampullae contractions are independent from heart activity and can drive
694 haemolymph flow (green arrows) by synchronized spatially restricted contractions (red
695 arrows) and dilatations (purple arrows)
696
697
698 **Fig. 3 Characterization of *B. leachii* haemocytes.** Stereotypical schemas along with
699 characteristic images of all haemocytes identified in *B. leachii* stained with Giemsa dye, both
700 from haemolymph smears and whole-colony histological sections. The illustrated cell is either
701 located at the centre of the image or indicated by an arrowhead. Note that the cells in the
702 histological sectioning show a degree of shrinkage following PFA fixation
703
704
705 **Fig. 4 Histology of palleal budding.** Abbreviations: zooid (z), first-generation bud (z_o),
706 second-generation bud (b), bud disc (b_d), oocyte (o), endostyle (e), pharyngeal basket (k),
707 stigmata (g), intestine (i), stomach (s). All sections are stained with H&E. (**A**) Typical *B. leachii*
708 asexual reproduction cycle with three generations co-existing: mature zooid (dark grey), two
709 first-generation buds (light grey) and two budlets visible. (**B**) Bud developing two bud discs
710 and oocytes. (**C**) First-generation bud with right budlet protruding and left budlet fully
711 circular. (**D**) Young bud starting to invaginate. (**E**) Older bud with pharyngeal basket, tentative
712 stigmata, a bud disc and oocytes. Arrowhead points at the interstitial space surrounding the
713 bud. (**F**) Bud on the point of becoming a filter-feeding zooid
714
715
716 **Fig. 5 Progression of *B. leachii* WBR.** Abbreviation: haemolymph clot (v_c), collagen (c_n),
717 spheroid bud (z_s), first-generation bud (z_o), intestine (i). (**A**) Stage 0: Giemsa stain of injured

718 vascular tissue displaying signs of tunic contraction (arrowheads) and clotting. (**B**) Stage 1:
719 Collagen remodelling and infiltration of cells into the tunic (arrowheads). Methyl blue within
720 MSB dyes collagen blue. (**C**) Stage 2: H&E stained giant cells (arrowheads) throughout the
721 remodelling vasculature. (**D**) Stage 3: Giemsa stained regeneration niches at different stages
722 of development, and increase in macrophage-like cells (see **A** and **F**). (**E**) Stage 4: H&E stain
723 shows competing regeneration niches at the first-generation and spheroid stages. (**F**) Stage 5:
724 Giemsa stain of a fully regenerated zooid with first-generation bud. (**G**) Evolution of
725 haemocyte types within ampullae throughout WBR, overlaid with the corresponding standard
726 error (dotted lines) and stages of WBR (see Fig. 1G). Cell types are indicated in the legend. The
727 color-coded asterisks show statistical significance between the corresponding populations
728 (Student's two-tailed *t*-test, *: $P < 0.05$, **: $P < 0.01$, ***: $P < 0.001$)
729

730 ## Electronic supplementary material

731

732 ### Supplementary figure legends

733

734

735 **Fig. S1 Quantification of haemolymph flow.** (**A**) Raw image overlaying the spatial margin
736 (black) used during the analysis. (**B**) Difference between **A** and its successor frame showing
737 moving haemocytes (white/red) and the added margin (magenta). (**C**) Detection of moving
738 cells thresholded from **B**. (**D**) Average detection of haemolymph movement inside vessels. (**E**)
739 Location of the main vessels thresholded from **D**. (**F**) Identified straight segments of vessels
740 (purple). (**G**) Difference frame used for tracking haemolymph flow. Start (blue) and end (red)
741 of objects' trajectories are visible. Dashed-delimited area magnified in **I**. (**H**) Difference frame
742 following that depicted in **G**. (**I**) Area magnified from **G**. (**J**) PIV quantification (green) of

743 haemolymph flow inferred using frames **G** and **H**. Dashed-delimited area magnified in **K**. (**K**)
744 Areas magnified from **J**. (**L**) 2D density histogram overlaying PIV measurements (dots),
745 inferred flow velocity (orange), smoothed velocity (brown) and the position of the frames
746 displayed in **A**-**K** (blue)
747
748
749 **Fig. S2 Quantification of ampullar contractions.** (**A**) Raw frame from the time-lapse
750 recording analysed in Fig. 2B. (**B**) Intensity-based thresholding of **A** used for the detection of
751 ampullae. (**C**) Detection of the ampullae in **A**, color-coded in shades of purple and overlaid
752 with centred circles of corresponding area. (**D**) Clustering of ampullar detections, color-coded
753 in shades of purple. Each circle depicts ampullar detection in some frame of the entire
754 recording. Coloured circles represent detections clustered together, black circles represent
755 spurious detections that were filtered out
756
757
758 **Fig. S3 Ampullar contraction induces haemolymph flow.** (**A**) Raw frame from the time-
759 lapse recording Movie S5. (**B**) Average difference between consecutive frames of the
760 recording. The blue-white-red colour-code depicts contraction in blue and dilatation in red.
761 (**C**) Average absolute second order difference between frames depicting haemolymph flow
762
763
764 **Fig. S4 Vascular lining detaching from the tunic in an adult colony.** High magnification of
765 a Giemsa stained histological section of a terminal ampulla in an adult colony. Arrows point a
766 portion of the vascular lining detaching from the surrounding tunic
767

Movie legends

Movie S1 Showcasing the various aspects of haemolymph flow in the vascular system of *B. leachii* vascular system using brightfield microscopy. Three different movies (from a large vessel, at a vascular junction and terminal ampullae, respectively) were combined to produce this presentation. The time and scale are specified on the frames of the recording in the top-left and bottom-right corners of the image, respectively. MPEG-4 recording file encoded with the H.264 codec

Movie S2 Haemolymph flow analysed in Fig. S1. MPEG-4 recording file encoded with the H.264 codec

Movie S3 The turbulences of haemolymph flow at junctions during flow reversal. The upper panel depicts the measured haemolymph velocity in the various vessel segments, while the lower panel overlays the original recording with the detected vessel segments (blue) and haemolymph flow (red arrows). MPEG-4 recording file encoded with the H.264 codec

Movie S4 Time-lapse recording of injury-induced WBR. MPEG-4 recording file encoded with the H.264 codec

Movie S5 Time-lapse recording of WBR, 6 days post injury. The recorded tissue is the one visible in Movie S4. MPEG-4 recording file encoded with the H.264 codec

792 **Table 1.** Summary of cell types present in the *Botrylloides leachii* circulatory system.

Cell type	Subtype	Circulatory cells	Older terminology
Undifferentiated cell [c, d]	Haemoblast [e, f]	Haemoblast [e, f] Differentiating cell	Lymphocyte [a, b] Stem cell [d]
Immunocyte [c]	Phagocyte [e]	Hyaline amoebocyte [d, f] Macrophage-like cell [d, f]	Amoebocytes with vacuole Signet ring cell [a, b] Vacuolated cell [c] Leukocyte [c]
	Cytotoxic cell [f]	Granular amoebocyte [b, d, f] Morula cell [b, d, e]	Cells with acidic vacuole [a] Green cell [b] Leukocyte [c] Vanadocyte [a]
Transport cell [e]	Granulocyte [e]	Compartment amoebocyte [d] Compartment cell [a, b, d]	Vacuolated cell [c]
Mast cell-like cell [d]	Granular cell [d]	Granular cell [d]	(Unique to *B. leachii*, [d])
Storage cell [f]	Vacuolated cell [f]	Pigment cell [a, c, d, e] Nephrocyte [c, d, e]	Cell with reflecting disks [a] Orange cell [b]

793
794 [a] (Endean, 1960); [b] (Freeman, 1964); [c] (Wright & Ermak, 1982); [d] (Cima et al., 2002); [e] (Hirose
795 et al., 2003); [f] (Ballarin et al., 2011)
796
797

798 **Table 2.** Classification chart of *Botrylloids leachii* haemocytes based on light microscopy
799 Giemsa stain. Only the most common traits are listed in this table, refer to Table S1 for full
800 description of the cell types.
801

Cell type	Size (µm)	Shape	Stain	Characteristic
Haemoblast	5 - 8	Round	Blue cytoplasm with a dark-blue nucleus	High nucleus to cytoplasm ratio
Differentiating cell	8 - 12	Swollen, irregular	Light-blue nucleus and grey cytoplasm	Fibrous cytoplasm with a proportionally large nucleus
Hyaline amoebocyte	6 - 9	Amoebocyte: highly irregular, including a variety of pseudopodia	Dual purple-blue cytoplasm	Purple stained clear cytoplasmic vesicles
Macrophage-like cell	6 - 20	Mostly round with irregular content	Blue with vesicles of varying shades of yellow, brown, green and grey	Vesicles highly heterogeneous in size, shape and content
Granular amoebocyte	6 - 10	Amoebocyte	Scattered dark-green cytoplasmic vesicles	Sparser vesicles than granular cells
Morula cell	10 - 16	Circular containing a low number of large (~2 µm), pale yellow and round vacuoles	Orange-green cytoplasmic colour in smears, red colour around the vacuoles in histological sections	Most common cell type in *B. leachii* haemolymph
Granular cell	8 - 12	Circular with irregular edge	Dense dark-blue/green vesicles	High density of vesicles renders the cell black and opaque
Compartment amoebocyte	7 - 10	Amoebocyte with a berry-like shape	Blue with a dark-blue nucleus	Numerous clear protruding vesicles
Compartment cell	12 - 18	Similar to morula	Unstained-grey opaque vesicles	Large uniform vesicles
Pigment cell	10 - 16	Similar to morula	Filled with minute dark granules, related to the colony colour	The content of the vesicle exhibits Brownian movement in living cells
Nephrocyte	10 - 16	Berry-like	Dark and speckled grey vesicles	An aggregate of dark grey vesicles

802
803

804 **Table S1**: Detailed description of haemolymph cell types present in the *B. leachii* vascular

Cell type (% of all haemocytes)	Description

805 system based on histological observations.

Undifferentiated cells	
Haemoblast	This small (5-8 µm), almost perfectly round, progenitor cell has a high nuclear-cytoplasmic ratio. It has a consistent dark blue nuclear stain, and most commonly a blue cytoplasmic stain. However, unstained or pink cytoplasmic staining was occasionally observed.
Differentiating cell (11 %)	A number of transitory cells can be identified in *B. leachii* haemolymph. Although it is difficult to determine which differentiation program these cells are following, the morphology of the majority of cells suggests that they originate from haemoblasts. These medium sized (8-12 µm) cells display a large light-blue stained nucleus, sometimes a nucleolus, and an unstained, often fibrous, grey cytoplasm with various morphological and staining features reminiscent of their future cell type.
Immunocytes	
Hyaline amoebocyte (3 %)	As with all other amoebocytes, this small (6-9 µm) cell has an irregular shape, typically displaying a large variety of pseudopodia. Hyaline amoebocytes have a dual purple-blue cytoplasmic staining, where the purple appears to originate from a variety of clear vesicles. In histological sections, both entirely purple cells and purple cells with a blue crescent containing the nucleus were observed.
Macrophage-like cell (19 %)	This extremely variable cell (6-20 µm) shows a wide range of sizes and shapes depending on the material it engulfed. Therefore, although most of the cells were fully stained dark-blue, some colour variations (including shades of yellow, brown, green and grey) were observed depending on the ingested material. Empty macrophage-like cells display a red crested cytoplasm (Cima et al., 2002). Particularly in large cells, the nucleus is displaced towards the periphery of the cell by the phagocytic vacuoles. While they can resemble compartment cells, macrophage-like cells have a greater heterogeneity in the size, shape and content of their vesicles.
Granular amoebocyte (1 %)	A small (6-10 µm) amoebocyte characterized by a number of scattered dark-green cytoplasmic vesicles. While they resemble granular cells, granular amoebocytes have a much lower density of granules, always displaying some portion of its cytoplasm. The cytoplasm is stained a light-blue/grey, although dark-blue and red have also been occasionally observed.
Morula cell (49 %)	This typically large (10-16 µm) cell is mostly characterized in smears by its orange-green cytoplasmic colour, and in histological sections by the red colour of the thin cytoplasm among the large vacuoles. It displays low numbers of large (~2 µm), pale yellow

	and round vacuoles, thus resulting in its characteristic berry-like shape.
Mast cell-like cells	
Granular cell (1 %)	A medium-sized (8-12 µm) cell, mostly circular, with a very irregular edge owing to the numerous small vesicles it contains. A variety of vesicles have been observed, but the majority are stained dark-blue/green and packed at such a high density that the whole cell appears black and opaque.
Transport cells	
Compartment amoebocyte (5 %)	A small (7-10 µm) amoebocyte characterized by numerous clear protruding vesicles, resulting in a berry-like shaped cell when observed unfixed. Its cytoplasm stains blue, with a dark blue nucleus easily visible in sections but harder to find in smears.
Compartment cell (4 %)	Large (12-18 µm) cell that displays few (typically less than 12) but large (~3 µm) opaque vesicles that remain mostly unstained-grey.
Storage cells	
Pigment cell (2 %)	A medium-sized (10-16 µm) cell that displays a number of large vacuoles filled with characteristic minute dark granules, whose colour relates to that of the colony (dark orange in this particular example).
Nephrocyte (1 %)	This medium-sized (10-16 µm) cell closely resembles pigment cells but lacks any pigment colour. These cells do not exhibit a circular shape filled with vesicles but rather a berry-like shape, as an aggregate of vesicles.

806
807
808

Figure 1

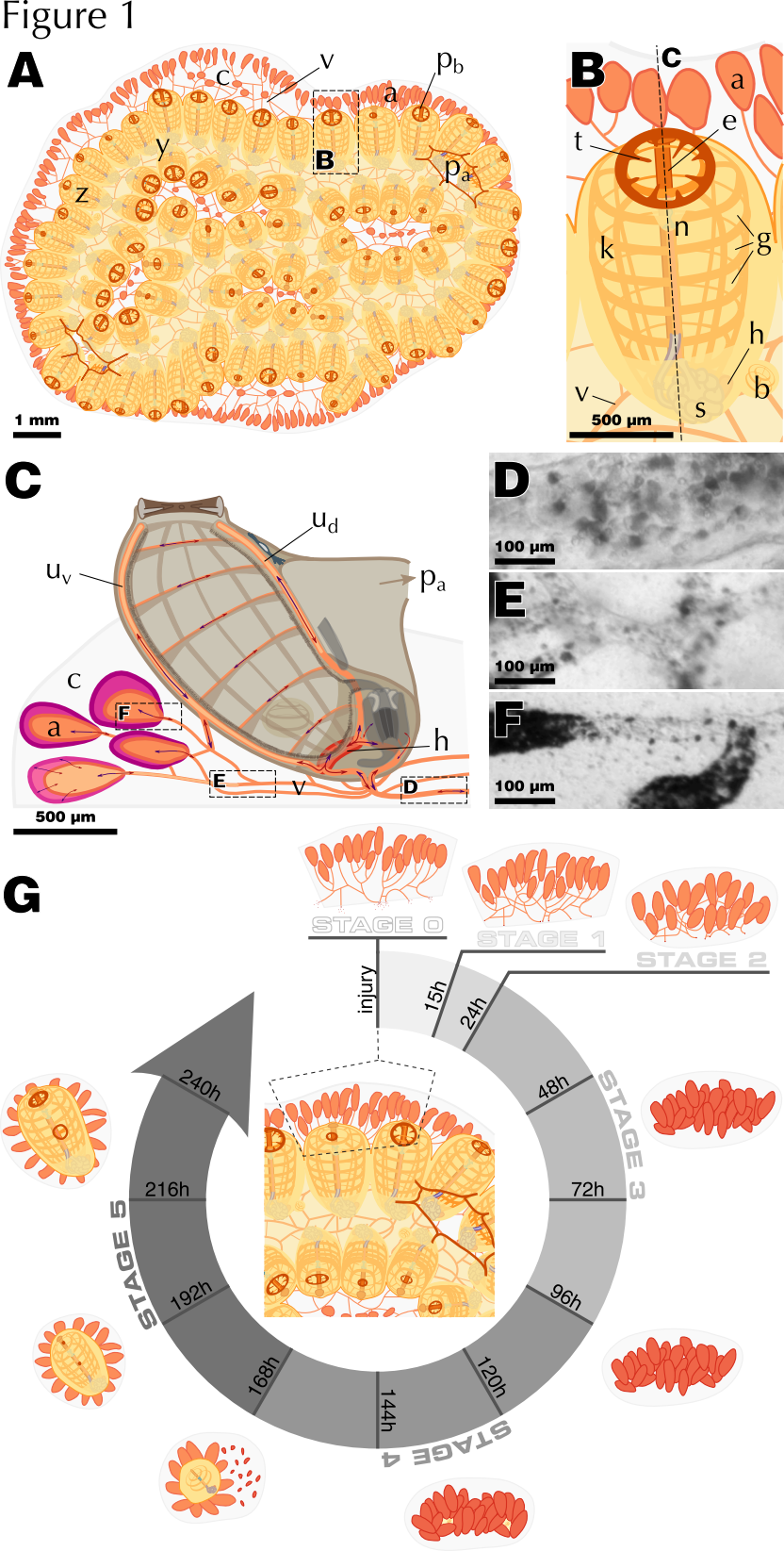
A
c
v
p_b
a
y
B
p_a
z
1 mm
B
c
a
e
t
n
k
g
h
b
v
s
500 µm
C
u_d
u_v
p_a
c
F
a
h
E
v
D
500 µm
D
100 µm
E
100 µm
F
100 µm
G
STAGE 0
STAGE 1
STAGE 2
injury
15h
24h
48h
STAGE 3
72h
96h
120h
144h
STAGE 4
168h
192h
216h
STAGE 5
240h

Figure 2

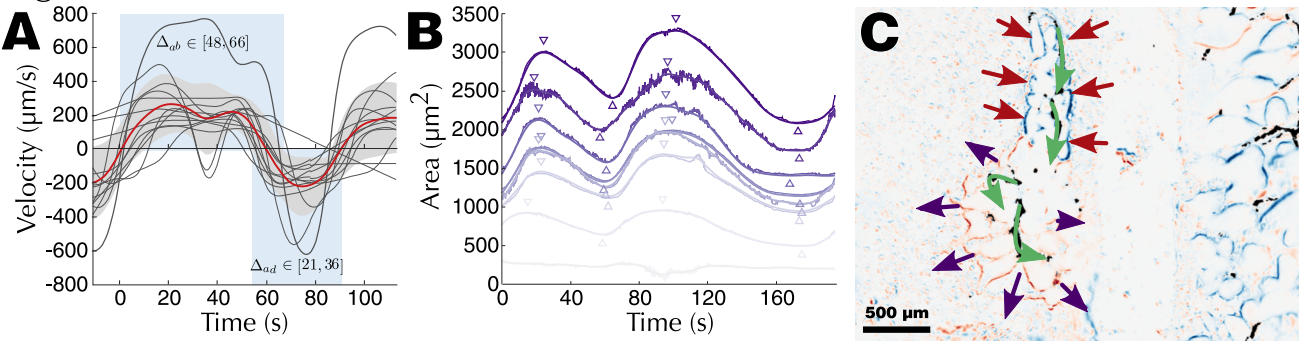
A
B
C
Velocity (μm/s)
Time (s)
$\Delta_{ab} \in [48, 66]$
$\Delta_{ad} \in [21, 36]$
Area (μm^2)
Time (s)
500 μm

Figure 3

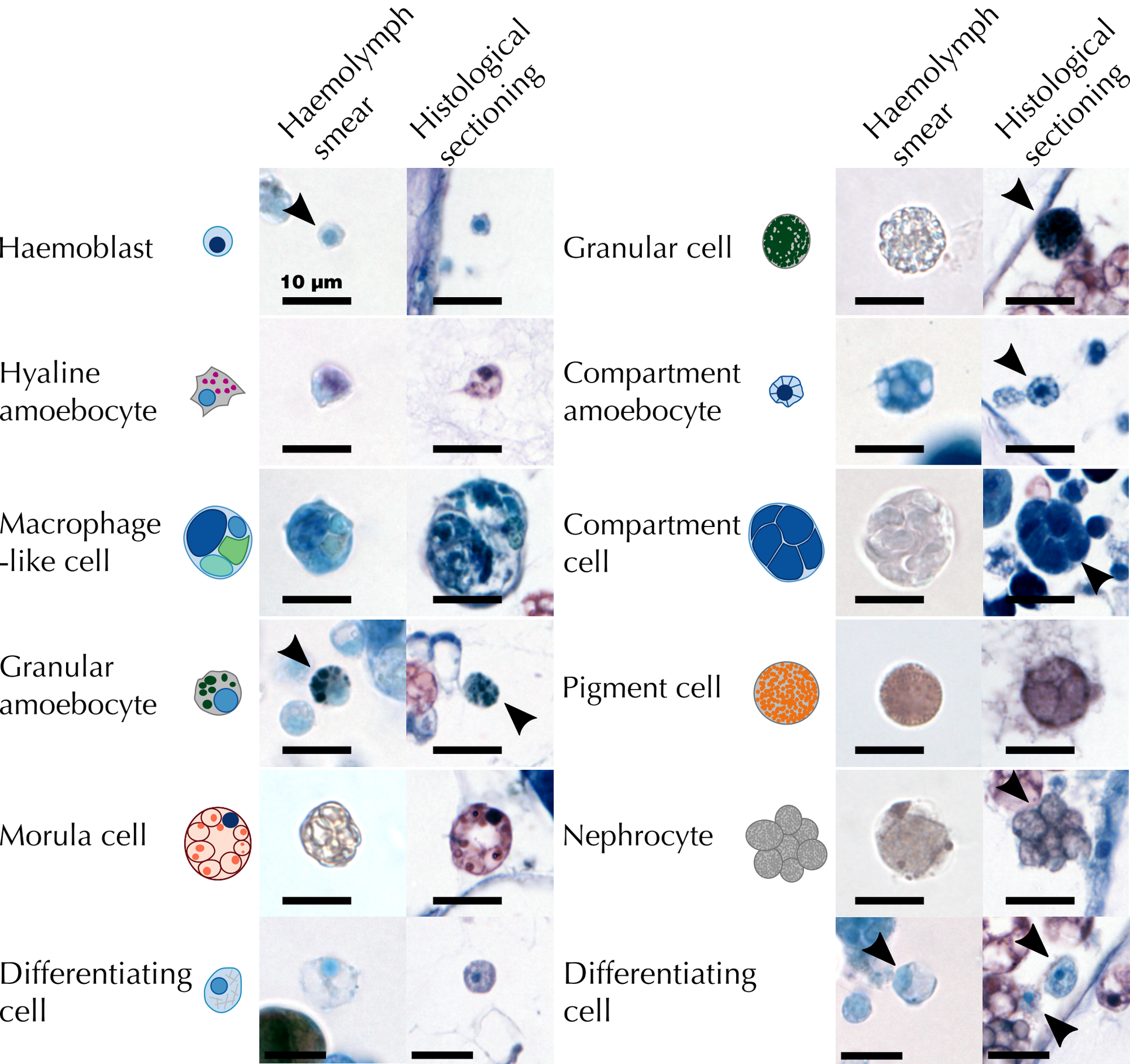
Haemolymph smear
Histological sectioning
Haemolymph smear
Histological sectioning
Haemoblast
10 µm
Granular cell
Hyaline amoebocyte
Compartment amoebocyte
Macrophage -like cell
Compartment cell
Granular amoebocyte
Pigment cell
Morula cell
Nephrocyte
Differentiating cell
Differentiating cell

Figure 4


A
b
z_o
b
z
z_o
100 µm

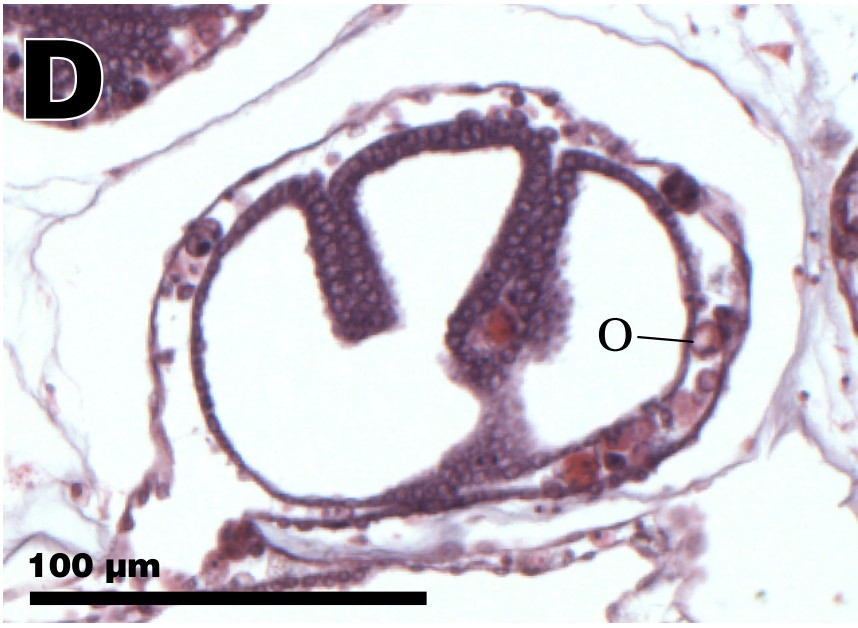
D
o
100 µm

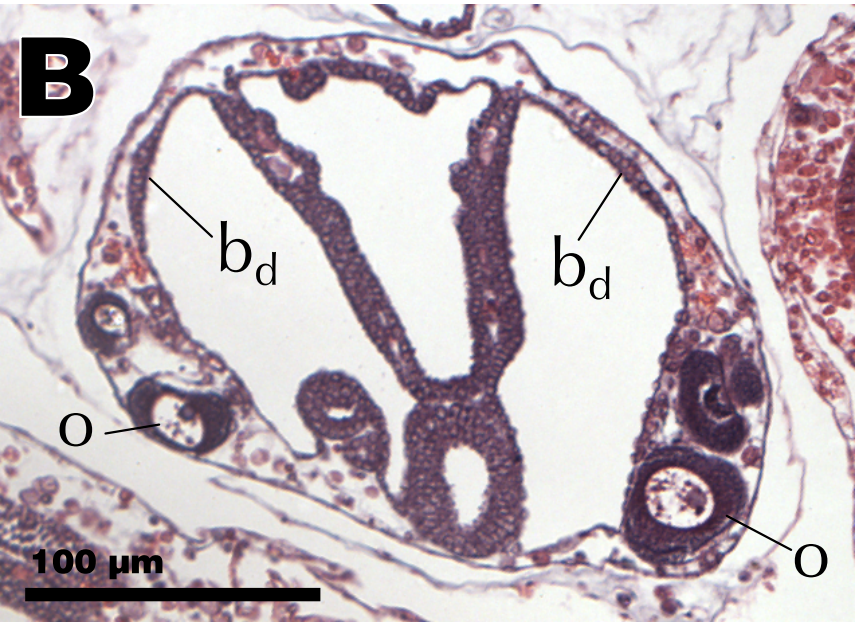
B
b_d
b_d
o
o
100 µm

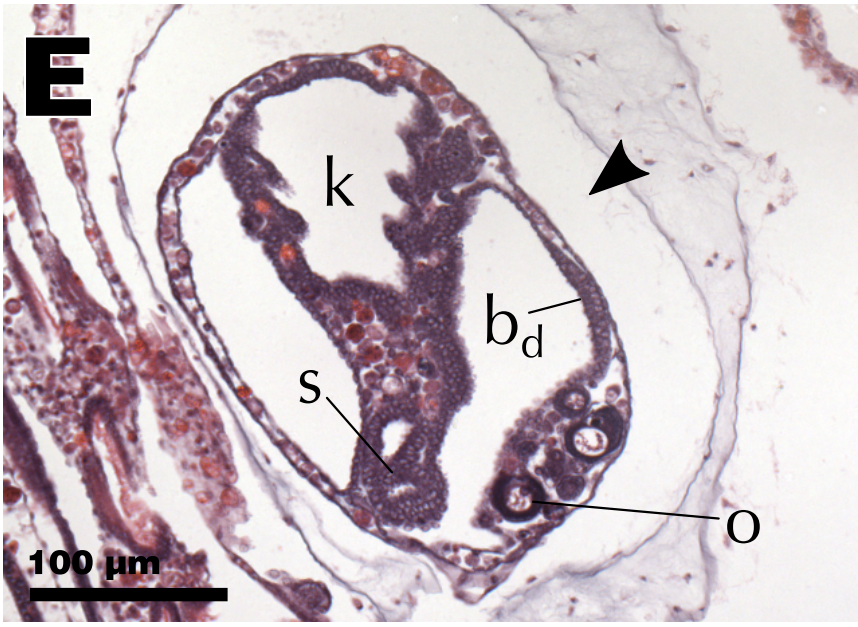
E
k
b_d
s
o
100 µm

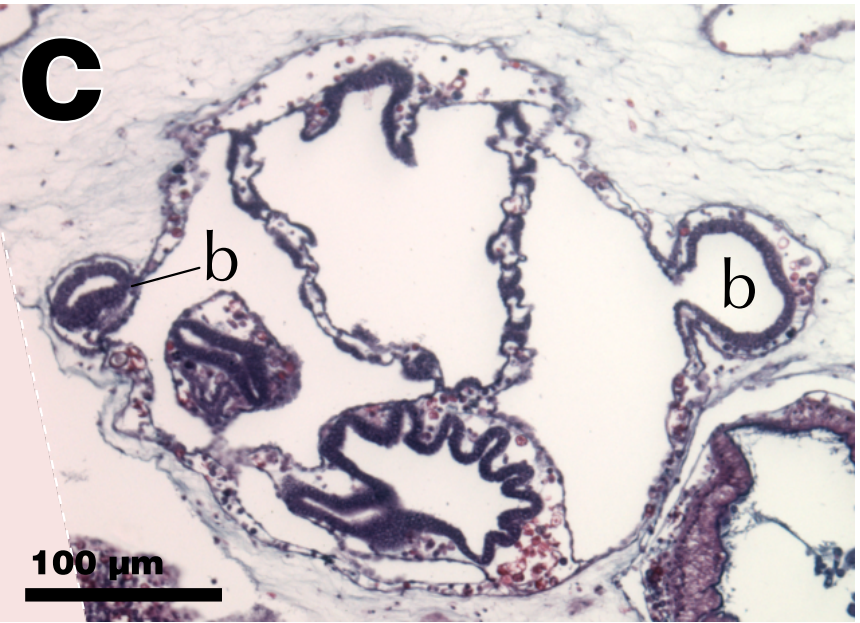
C
b
b
100 µm

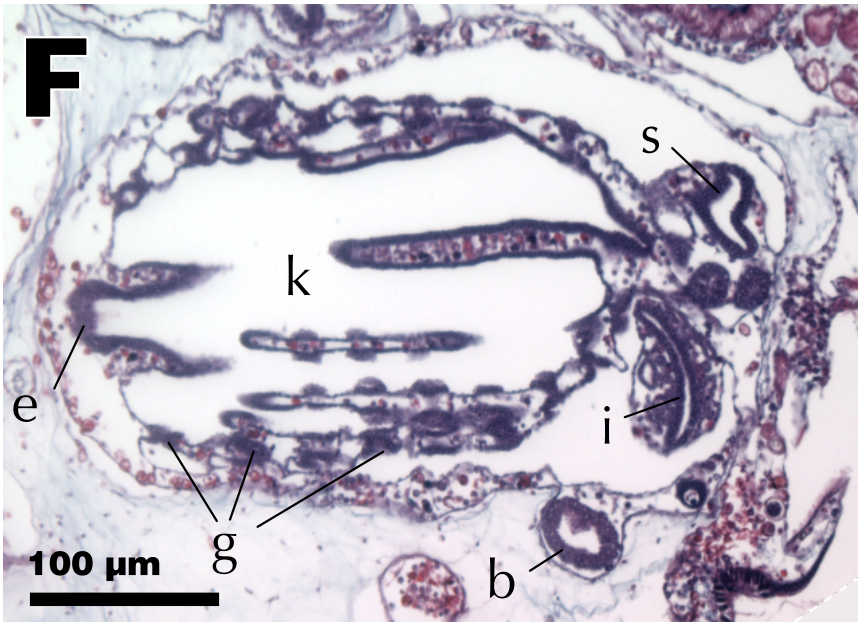
F
s
k
e
i
g
b
100 µm

Figure 5

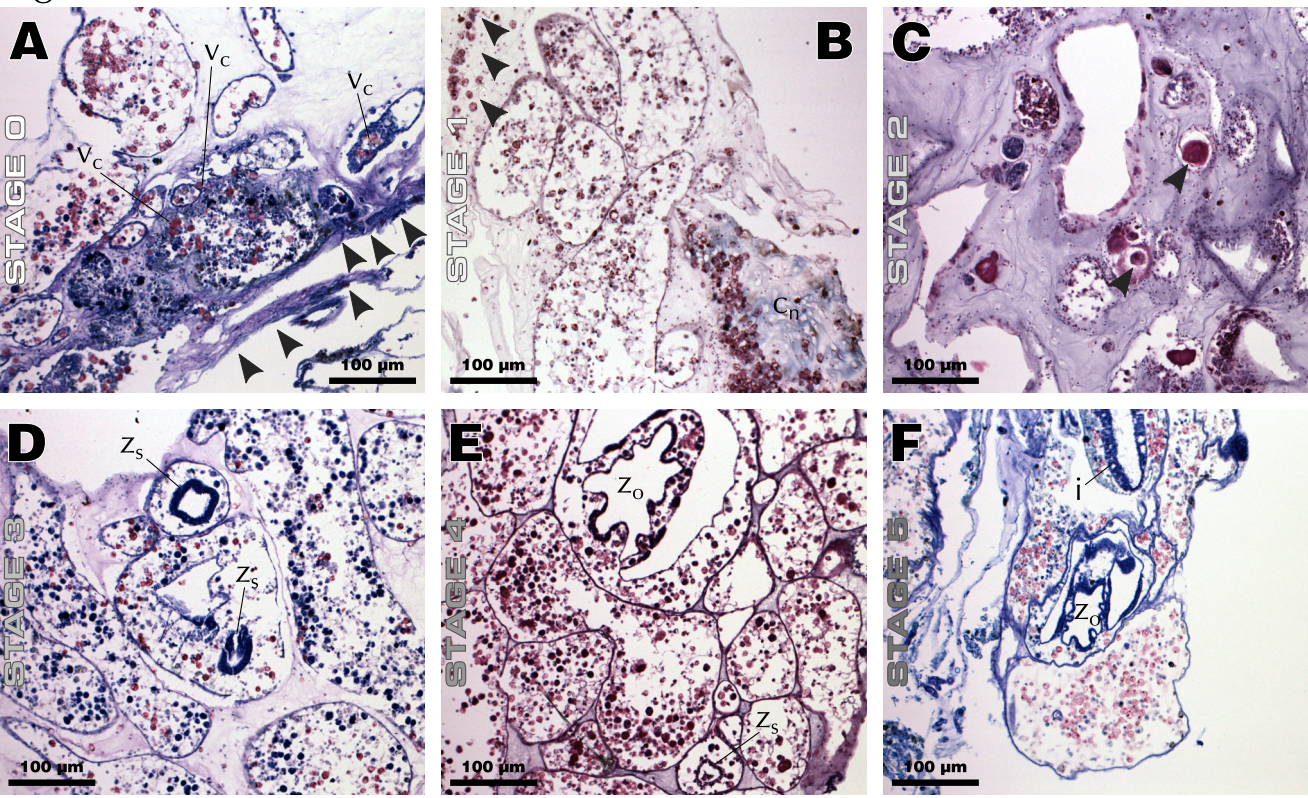
A
STAGE 0
V_C
V_C
V_C
100 µm
B
STAGE 1
C_n
100 µm
C
STAGE 2
100 µm
D
STAGE 3
Z_S
Z_S
100 µm
E
STAGE 4
Z_O
Z_S
100 µm
F
STAGE 5
i
Z_O
100 µm

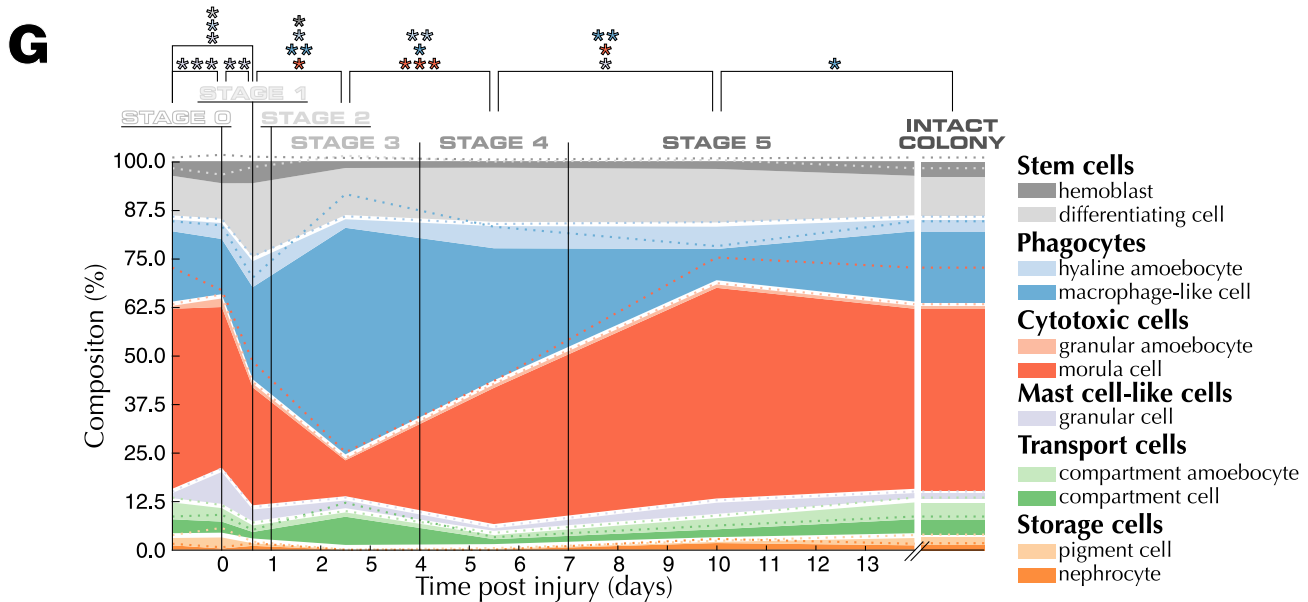
G
STAGE 0
STAGE 1
STAGE 2
STAGE 3
STAGE 4
STAGE 5
INTACT COLONY
100.0
87.5
75.0
62.5
50.0
37.5
25.0
12.5
0.0
Compositon (%)
0
1
2
5
4
5
6
7
8
9
10
11
12
13
Time post injury (days)
Stem cells
hemoblast
differentiating cell
Phagocytes
hyaline amoebocyte
macrophage-like cell
Cytotoxic cells
granular amoebocyte
morula cell
Mast cell-like cells
granular cell
Transport cells
compartment amoebocyte
compartment cell
Storage cells
pigment cell
nephrocyte